A wavenumber approach to analysing the active control of plane waves with arrays of secondary sources

Stephen J. Elliott[a], Jordan Cheer[a], Lam Bhan[b], Chuang Shi[c], Woon-Seng Gan[b]

[a]*Institute of Sound and Vibration Research, University of Southampton, Highfield, Southampton, SO17 1BJ*
[b]*Digital Signal Processing Lab, School of Electrical & Electronic Engineering, Nanyang Technological University, Singapore*
[c]*School of Electronic Engineering, University of Electronic Science and Technology of China, Chengdu, Sichuan, China*

Abstract

The active control of an incident sound field with an array of secondary sources is a fundamental problem in active control. In this paper the optimal performance of an infinite array of secondary sources in controlling a plane incident sound wave is first considered in free space. An analytic solution for normal incidence plane waves is presented, indicating a clear cut-off frequency for good performance, when the separation distance between the uniformly-spaced sources is equal to a wavelength. The extent of the near field pressure close to the source array is also quantified, since this determines the positions of the error microphones in a practical arrangement. The theory is also extended to oblique incident waves. This result is then compared with numerical simulations of controlling the sound power radiated through an open aperture in a rigid wall, subject to an incident plane wave, using an array of secondary sources in the aperture. In this case the diffraction through the aperture becomes important when its size is compatible with the acoustic wavelength, in which case only a few sources are necessary for good control. When the size of the aperture is large compared to the wavelength, and diffraction is less important but more secondary sources need to be used for good control, the results then become similar to those for the free field problem with an infinite source array.

Keywords: Active noise control, Feedforward control, Wavenumber domain

1. Introduction

The active control of an incident sound field inside a closed surface using a discrete array of secondary sources has been considered using numerical models in the 2-D case of a circle by Zavadskaya et al [1] and in the 3-D case of a sphere by Konyaev et al [2]. The secondary sources were assumed to be combinations of point monopoles and dipoles, as described by Mangiante [3] for example as a Huygens' source, regularly arranged to control the sound inside the surface without external radiation. It was found in both the 2-D and the 3-D studies [1, 2] that the spacing between the secondary sources, required to achieve a good level of control within the closed surface needed to be closer than about $\lambda/2$, where λ is the acoustic wavelength, as noted by Nelson and Elliott [4].

It might be expected that as the radius of the surface becomes very large, the problem would reduce to that of the control of an incident plane wave by an infinite array of secondary sources normal to the direction of propagation. It is shown below, however, that perfect control of such a normally-incident plane wave can be achieved with an infinite array having a separation of λ, rather than $\lambda/2$. This analysis is best performed using a wavenumber decomposition of the secondary source array and subsequent sound radiation, and this wavenumber analysis can be extended to plane waves that are not normal to the array, both in 2-D and in 3-D.

Although it is of fundamental interest to analyse the limits to the performance of such an array, it potentially has applications in sound reproduction and in the active control of environmental noise. It becomes more difficult to analyse the performance when the size of the array is finite, although this case is applicable to the active control of sound transmitted through open windows, as considered, for example, by Murao and Nishimura [5], Lam *et al* [6] and Wang *et al* [7]. The analytic results for an infinite array are therefore compared with the results from a numerical simulation of active control in this application.

A preliminary version of this paper with a less general formulation for the active control was presented by Elliott *et al* [8], and some of the numerical simulations in Section 6 were presented by Bhan *et al* [6].

Email address: s.j.elliott@soton.ac.uk (Stephen J. Elliott)

2. Control of a normally-incident plane wave with an infinite array of secondary sources in 2-D

In order to easily illustrate the method, we begin by considering the active control of a normally-incident plane wave in free space using an infinite 2-D array of secondary sources. This arrangement is illustrated in Figure 1a, where the objective is to suppress the incident primary wave to the right of the array of line sources in the plane of the figure. If the aim was to actively absorb the incident wave, each of the secondary sources would need to be a combination of a monopole and a dipole, arranged such that the sound radiation to the left of the array was minimised. The problem to the right of the array, however, is similar to that if the secondary sources were only assumed to be monopoles, although in this case the secondary source array would reflect the incident wave and so the sound field to the left of the array would consist of a standing wave, due to the interference between the incident and a reflected wave, as it does for a plane wave in a duct controlled with a single secondary source [4]. In order to provide generality, and extension to the control of oblique waves in Section 4, a wavenumber analysis of the problem is presented here, although in an earlier conference publication [8] the control of a normally-incident plane wave was analysed using an analogous duct formulation [9].

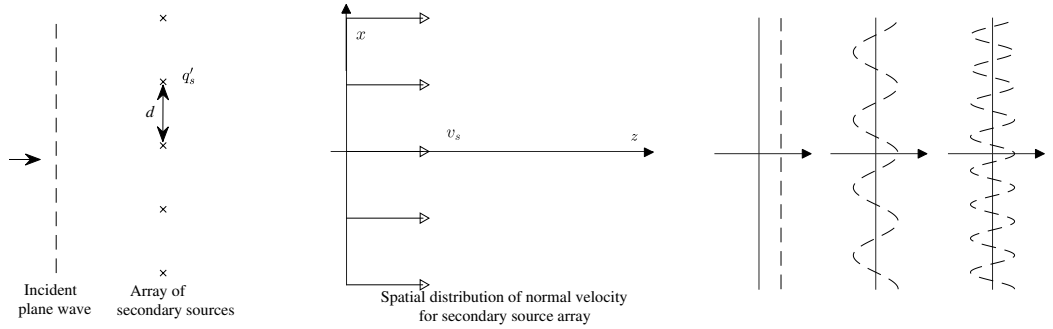

Figure 1: Physical arrangement in 2-D of an incident plane wave being controlled to the right of an infinite array of secondary line sources in the plane of the figure (a). Also shown (b) is the spatial distribution of the normal velocity for a section of the secondary source array and the first three spatial harmonics of its wavenumber decomposition (c).

We assume a primary plane wave of the form

$$p_p(z) = p_p \mathrm{e}^{-\mathrm{j}k_0 z}, \tag{1}$$

where z is the direction normal to the array, as shown in Fig. 1 k_0 is ω/c_0, c_0 is the speed of sound and p_p is the complex pressure proportional to $\mathrm{e}^{\mathrm{j}\omega \mathrm{t}}$. The normal particle velocity associated with this wave is

$$v_p(z) = \frac{p_p}{\rho_0 c_0} \mathrm{e}^{-\mathrm{j}k_0 z}, \tag{2}$$

where ρ_0 is the density of the medium. To control this primary field we assume an infinite array of secondary line sources, uniformly separated by a distance d in the x direction, which must all have equal source strengths, by symmetry. If each secondary source strength per unit length is q_s', then the normal particle velocity associated with the secondary sources when z is equal to zero is

$$v_s(x, 0) = q_s' \sum_{m=-\infty}^{\infty} \delta(x - md), \tag{3}$$

where δ is the Dirac delta function and m is the secondary source index. Taking the Fourier series of $v_s(x, 0)$ gives

$$v_s(x, 0) = \frac{q_s'}{d} \sum_{n=-\infty}^{\infty} \mathrm{e}^{\mathrm{j}2\pi n x/d}, \tag{4}$$

where q_s'/d has the dimensions of a linear velocity and can be written as v_s. The Fourier series can also be written in terms of the wave numbers k_{xn}, equal to $2\pi n/d$, as

$$v_s(x, 0) = v_s \left[1 + 2 \sum_{n=1}^{\infty} \cos(k_{xn} x) \right]. \tag{5}$$

The secondary source velocity distribution, eq. (3), is shown in Figure 1b, together with the first 3 terms of the Fourier series in eq. (5). This velocity distribution will propagate in the z direction so that in general [10]

$$v_s(x, z) = v_s \left[\mathrm{e}^{-\mathrm{j}k_0 z} + 2 \sum_{n=1}^{\infty} \cos(k_{xn} x) \mathrm{e}^{-\mathrm{j}k_{zn} z} \right]. \tag{6}$$

where the wavenumber in the z direction for the n-th spatial harmonic is

$$k_{zn} = \sqrt{k_0^2 - k_{xn}^2}. \tag{7}$$

At frequencies for which $k_0 < k_{x1}$, i.e. $f < \frac{c_0}{d}$, where f is the frequency in hertz, only the zeroth-order term in the Fourier series propagates, since k_{zn} is imaginary for all other n and so these terms are evanescent. When $k_{x1} > k_0 < k_{x2}$, i.e. $\frac{c_0}{d} < f < \frac{2c_0}{d}$, both the zeroth and first terms propagate, since k_{x1} is then also real.

Figure 2a shows the number of higher-order terms in the Fourier series that can propagate, as a function of normalised frequency kd, together with the real parts of k_{zn} in each case (Figure 2b). The total normal particle velocity due to both the primary and secondary sources is thus

$$v_T(x,z) = \left(\frac{p_p}{\rho_0 c_0} + v_s\right) \mathrm{e}^{-\mathrm{j}k_0 z} + 2v_s \sum_{n=1}^{\infty} \cos(k_{xn}x)\mathrm{e}^{-\mathrm{j}k_{zn}z}. \tag{8}$$

Using the conservation of momentum equation, the pressure associated with the normal velocity distribution at the secondary source array can be written as [10]

$$p_s(x,0) = \rho_0 c_0 v_s \left[1 + 2\sum_{n=1}^{\infty} \frac{k_0}{k_{zn}} \cos(k_{xn}x)\right], \tag{9}$$

which also propagates in the z direction to give

$$p_s(x,z) = \rho_0 c_0 v_s \left[\mathrm{e}^{-\mathrm{j}k_0 z} + 2\sum_{n=1}^{\infty} \frac{k_0}{k_{zn}} \cos(k_{xn}x)\mathrm{e}^{-\mathrm{j}k_{zn}z}\right]. \tag{10}$$

The total pressure due to the primary and secondary sources is thus

$$p_T(x,z) = (p_p + \rho_0 c_0 v_s)\, \mathrm{e}^{-\mathrm{j}k_0 z} + 2\rho_0 c_0 v_s \sum_{n=1}^{\infty} \frac{k_0}{k_{zn}} \cos(k_{xn}x)\mathrm{e}^{-\mathrm{j}k_{zn}z} \tag{11}$$

The acoustic intensity normal to the array is

$$I(x,z) = \frac{1}{2}\Re\left[p_T^*(x,z)v_T(x,z)\right], \tag{12}$$

where $\Re$ denotes the real part of the complex quantity in square brackets and * denotes complex conjugation. Integrating this from $x = 0$ to $x = d$, the spatially-averaged intensity is

$$\Pi(x,z) = \frac{1}{2}\Re\left[\int_0^d p_T^*(x,z)v_T(x,z)\mathrm{d}x\right]. \tag{13}$$

Using equations (8) and (11), and the orthogonality of the cosine functions, this can be written as

$$\Pi(x,z) = \frac{1}{2}\left(p_p^* + \rho_0 c_0 v_s^*\right)\left(\frac{p_p}{\rho_0 c_0} + v_s\right) + \rho_0 c_0 |v_s|^2 \Re\sum_{n=1}^{\infty}\frac{k_0}{k_{zn}}\mathrm{e}^{-\mathrm{j}(k_{zn}-k_{zn}^*)z}. \tag{14}$$

At the 'cut-on' frequency for the n-th spatial harmonic, k_{xn} is equal to k_0, so that k_{zn} in eq. (7) is zero. The dependence of the intensity on $1/k_{zn}$ in eq. (14) would give rise to singularities in this quantity if v_s were finite at the cut-on frequency, as illustrated in Figure 9.10 in [11] for example. So, at any given frequency, only some of the spatial harmonics can propagate, when k_{zn} is real, in which case $k_{zn} - k_{zn}^*$ is zero and $\mathrm{e}^{-\mathrm{j}(k_{zn}-k_{zn}^*)z}$ is unity. The higher order spatial harmonics are evanescent, and so since k_{zn} is imaginary, $\Re\{k_0/k_{z_n}\}$ is zero.

We now define a cost function to be minimised, J, equal to $2\Pi(x,z)$, which is given by

$$J = \left(p_p^* + \rho_0 c_0 v_s^*\right)\left(\frac{p_p}{\rho_0 c_0} + v_s\right) + 2\rho_0 c_0 |v_s|^2 \Re\sum_{n=1}^{L}\frac{k_0}{k_{zn}}, \tag{15}$$

where the summation is only taken over the L higher order spatial harmonics that generate a propagating acoustic field, at a given frequency, and $\Re$ again denotes the real part and is introduced to avoid including the $n = 1$ term before k_{z1} becomes real. This cost function can be written in Hermitian quadratic form

$$J = v_s^* A v_s + b^* v_s + v_s^* b + c \tag{16}$$

where

$$A = \rho_0 c_0\left(1 + 2\Re\sum_{n=1}^{L}\frac{k_0}{k_{zn}}\right) \tag{17}$$

$$b = p_p \tag{18}$$

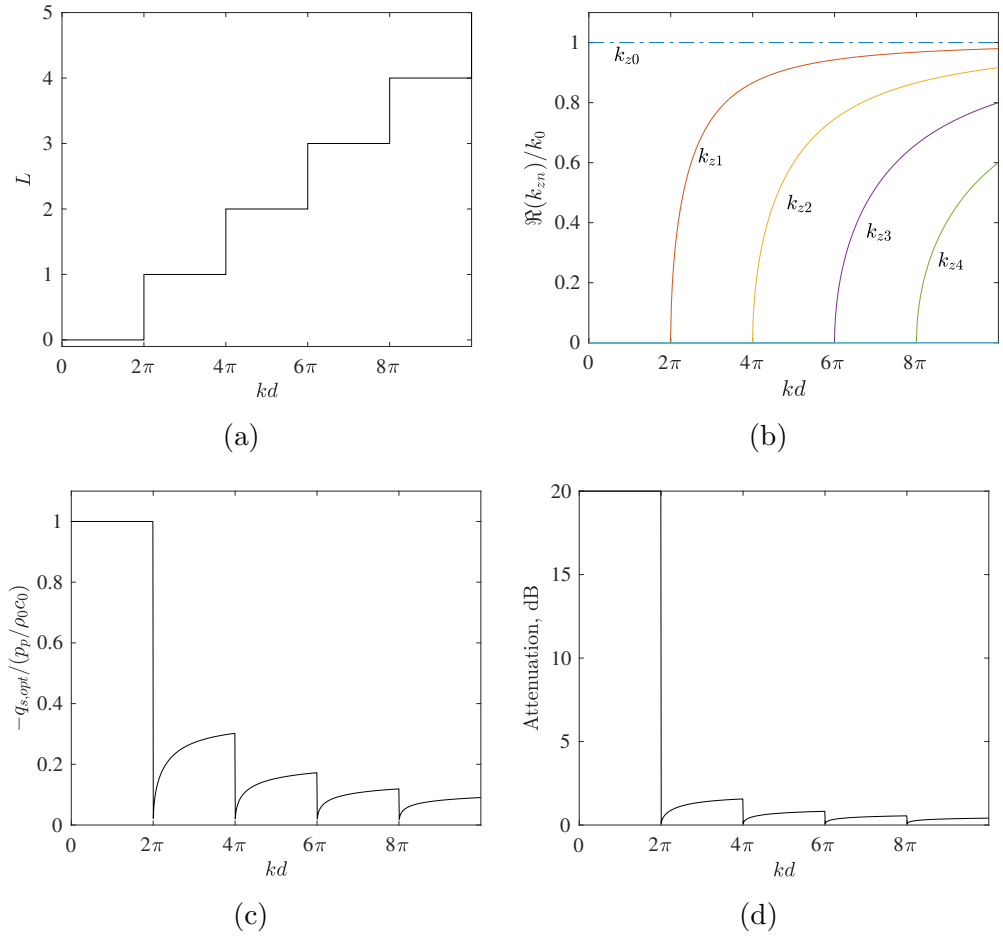

Figure 2: The number of higher-order spatial harmonics that can propagate, L, as a function of normalised frequency, kd, equal to $2\pi d/\lambda$ (a), together with the real parts of the corresponding wavenumbers in the propagating direction (b). The optimal secondary source velocity is also shown (c) together with the attenuation in the primary field (d).

and

$$c = \frac{|p_p|^2}{\rho_0 c_0}. \tag{19}$$

This cost function is minimised if the secondary source strength corresponds to

$$v_{s,opt} = \frac{-p_p/\rho_0 c_0}{\left(1 + 2\Re \sum_{n=1}^{L} \frac{k_0}{k_{zn}}\right)}, \tag{20}$$

in which case the attenuation in the power can be written as

$$\text{Atten} = -10 \log_{10} \frac{J_{\min}}{c}, \tag{21}$$

where

$$J_{\min} = c - |b|^2/A. \tag{22}$$

The optimal secondary source strength and predicted attenuation are plotted in Figures 2c and 2d respectively, and show that below the first cut-on frequency, at $f = c_0/d$, the secondary source strength is constant. The attenuation is, in principle, infinite below this frequency but drops to zero when the frequency is exactly c_0/d, since the secondary source strength is then zero to avoid the singularity referred to above. Although the optimum value of the secondary source strength is generally finite above this frequency, the attenuation is small.

3. Positioning of error sensors

The optimum source strength in eq. (20) has been derived by minimising the total acoustic power transmitted past the secondary source array. A practical system, however, would probably operate by minimising the sum of the squared outputs of an array of error microphones and so it is of interest to calculate how far this error microphone array must be from the secondary source array to achieve good control.

Figure 3 shows the magnitude of the sound pressure level after active control in the 2-D case, with the source strengths given by eq. (20). The pressure field to the right of the secondary source array is calculated using eq. (11). For completeness, the pressure field to the left of the secondary source array is also shown and is calculated from

$$p_T(x,z)|_{z<0} = p_p \mathrm{e}^{-\mathrm{j}k_0 z} + \rho_0 c_0 v_s \mathrm{e}^{\mathrm{j}k_0 z} + 2\rho_0 c_0 v_s \sum_{n=1}^{\infty} \frac{k_0}{k_{zn}} \cos(k_{xn} x) \mathrm{e}^{\mathrm{j}k_{zn} z}. \tag{23}$$

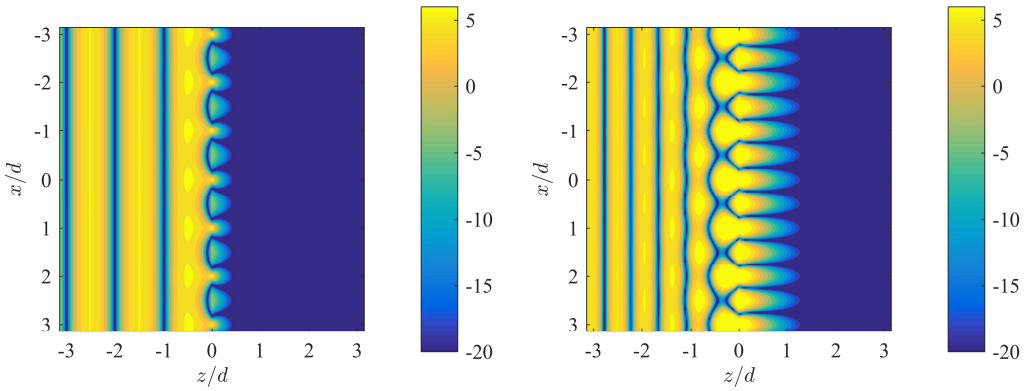

(a) (b)

Figure 3: The sound pressure level, in dB relative to the incident pressure, after active control with an infinite array of secondary sources in the 2-D case, where the secondary source strengths are adjusted using eq. (20), for $k_0 d$ equal to π (a) and 1.8π (b) corresponding to source separation distances of 0.5λ and 0.9λ.

The pressure field to the right of the secondary sources after control is characterised by "tongues" of high pressure eminating from each secondary source, caused by the evanescent decay of the higher order spatial harmonics. Similar tongues of pressure are seen for the reproduction of plane waves using wave field synthesis, WFS, and analysed using a similar wavenumber decomposition in [12] and [13]. This near-field pressure extends further to the right in Figure 3 at higher frequencies and is dominated by the evanescent decay of the first higher order spatial harmonic, which, for $k_0 < 2\pi/d$, has an imaginary axial wavenumber of

$$k_{z1} = -\mathrm{j}\sqrt{\left(\frac{2\pi}{d}\right)^2 - k_0^2}. \tag{24}$$

This harmonic has thus decayed by 20 dB when

$$\frac{z}{d} = \frac{\ln(10)}{\sqrt{(2\pi)^2 - (k_0 d)^2}}, \tag{25}$$

which has a limiting low frequency value of about 0.37, and this distance is plotted as a function $k_0 d$ in Figure 4. This gives an indication of the

minimum distance between the secondary sources and the error microphones for control performance of at least 20 dB.

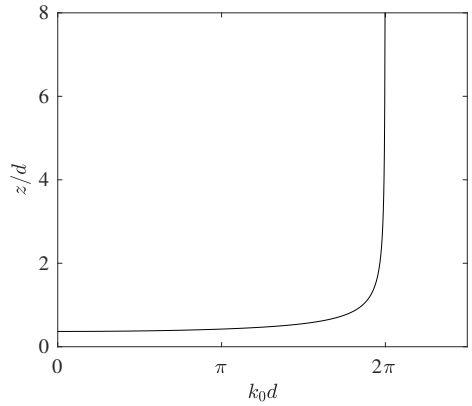

Figure 4: The minimum distance of the error microphones from the secondary source array for 20 dB attenuation of the evanescent field. This tends to infinity when $d = \lambda$ and does not exist for frequencies above this limit.

After the evanescent field has decayed away, it is clear from Figure 3 that, to the left of the array, a standing wave is formed between the forward-going incident plane wave and the backwards-going plane wave generated by the secondary source array. The monopole secondary sources essentially reflect the incident wave, as does a single secondary source in a duct [4]. A combination of monopoles and dipoles can be used to absorb the incident wave [3], as noted in the introduction. In practice, pairs of loudspeakers could be used to synthesise the effect of a monopole and a dipole source arrangement [4]. These could either be implemented with two separate loudspeaker drivers, which are more efficient if they share an enclosure [14], or a single loudspeaker driver in a phase-shift enclosure [15, 16, 17, 18]. It is interesting to examine the near field contribution of such pairs of sources, in comparison with the monopole above, since this again determines the minimum spacing of an array of error sensors from the secondary source array.

Consider the sound field due to the array shown in Figure 5 when controlling a normally incident plane wave. The source strength of all the secondary sources in each of the two layers are the same, by symmetry. The left-hand layer of secondary sources, with volume velocity per unit length of q'_{s2}, must, however, be arranged to cancel out the backward going plane wave from the right-hand layer of secondary sources, with volume velocity per unit length

q'_{s1}.

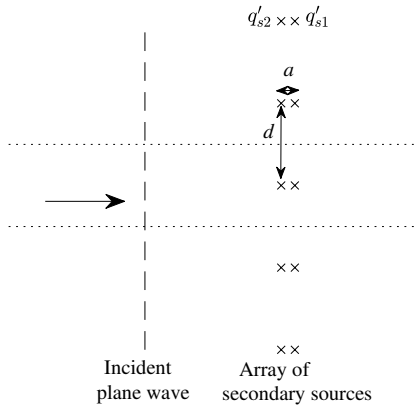

Figure 5: Arrangement of an array of secondary source pairs used to absorb a normally-incident plane wave.

Two hypothetical planes, normal to the array of secondary sources, and placed at the mid-point on either side of one pair of sources, are also shown in Figure 5. By symmetry, the particle velocity in the direction parallel to the line of the sources must be zero on these planes and so they can be considered as the sides of an infinite 2D duct [8]. The condition that the backward going plane wave is suppressed is thus the same as in the analogous problem of active control in a duct [4], i.e.,

$$v_{s2} = -v_{s1}\mathrm{e}^{-\mathrm{j}k_0 a}, \tag{26}$$

where $v_{s1} = q'_{s1}/d$ and $v_{s2} = q'_{s2}/d$ and a is the distance between the two layers of secondary sources. The plane-wave pressure generated in the forward going direction is thus

$$p_{s0}(z) = \rho_0 c_0 v_{s1} \left(1 - \mathrm{e}^{-\mathrm{j}2k_0 a}\right) \mathrm{e}^{-\mathrm{j}k_0 z}. \tag{27}$$

Setting this equal to $-p_p \mathrm{e}^{-\mathrm{j}k_0 z}$ gives the value of v_{s1} required for plane wave control, when $f < c_0/d$,

$$v_{s1,opt} = \frac{-p_p}{\rho_0 c_0 (1 - \mathrm{e}^{-\mathrm{j}2k_0 a})}. \tag{28}$$

Using this and v_{s2} given by eq. (26), again allows the total pressure field around the secondary sources to be calculated, and this is plotted in Figure 6, in which a is assumed to be $d/10$.

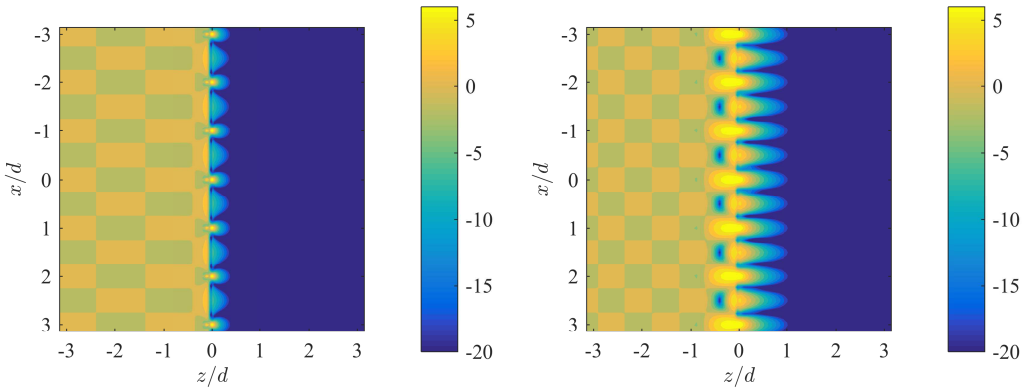

(a) (b)

Figure 6: The sound pressure level, in dB relative to the incident field, after active control with an infinite array of secondary sources arranged in 2 layers, as show in Figure 5 in the 2-D case, where the secondary source strengths are adjusted using eqs. (26) and (28), for $k_0 d$ equal to π (a) and 1.8π (b), corresponding to source separation distances of 0.5λ and 0.9λ.

Provided a is not too small compared with the wavelength, the magnitude of the term $(1 - \mathrm{e}^{-\mathrm{j}2k_0 a})$ in eq. (28) will not be too much smaller than unity, so the magnitudes of the source strengths in this two-layer array will not be too much greater than those in the single layer array. This explains why the extent of the near-fields in Figures 3 and 6 are similar and suggests that the guidelines for the error sensor positioning given in eq. 25 is still useful, assuming again that $k_0 a$ is not too small. The sound field to the left of the double-layer array in Figure 6 is almost uniform, since the array is absorbing the incident wave in this case, as in the original formulation in [1, 2].

4. Control of an oblique plane wave with an infinite array of secondary sources in 2-D

Returning to active control with a single layer of monopole secondary sources, we now assume that the primary field is generated at an oblique angle, θ, in the 2-D geometry shown in Figure 2a, in which case its pressure field is

$$p_p(x, z) = p_p \mathrm{e}^{-\mathrm{j}k_0(x \sin\theta + z \cos\theta)} \tag{29}$$

and the particle velocity in the normal direction becomes

$$v_p(x,z) = \frac{p_p \cos\theta}{\rho_0 c_0} \mathrm{e}^{-\mathrm{j}k_0(x\sin\theta + z\cos\theta)}. \tag{30}$$

In order to control this primary field, the elements of the secondary source array must have an appropriate phase shift, equal to $k_0 md \sin\theta$. Writing md as x, the normal velocity distribution due to the secondary source array can thus be written as

$$v_s(x,0) = q_s' \sum_{n=1}^{\infty} \delta(x - md) \mathrm{e}^{-\mathrm{j}k_0 x \sin\theta}. \tag{31}$$

Taking the spatial Fourier transform of $v_s(x,0)$ gives

$$v_s(x,0) = v_s \sum_{n=-\infty}^{\infty} \mathrm{e}^{\mathrm{j}(2\pi n x/d - k_0 x \sin\theta)} \tag{32}$$

and assuming that k_{xn} is equal to $2\pi n/d$, as above,

$$v_s(x,0) = v_s \mathrm{e}^{-\mathrm{j}k_0 x \sin\theta} \left[1 + 2 \sum_{n=1}^{\infty} \cos(k_{xn} x) \right]. \tag{33}$$

Figure 7 shows the positions of these spatial harmonics in k-space [10], together with a radiation circle of radius k_0 when the frequency is just below c_0/d Hz. In the case where θ is equal to 0, only one spatial harmonic, at $k_x = 0$, would be able to propagate at this frequency, but assuming $\theta > 0$, there is now an additional spatial harmonic that can radiate when

$$\frac{2\pi}{d} - k_0 \sin\theta = k_0, \tag{34}$$

i.e.

$$k_0 = \frac{2\pi}{d(1 + \sin\theta)} \qquad \text{for} \quad \theta > 0. \tag{35}$$

If $\theta < 0$, it is the higher order spatial harmonic, originally at $-2\pi/d$, that first starts to radiate, when

$$-\frac{2\pi}{d} + k_0 \sin\theta = -k_0 \tag{36}$$

i.e.

$$k_0 = \frac{2\pi}{d(1-\sin\theta)} \qquad \text{for} \quad \theta < 0. \tag{37}$$

So the general condition for this first higher order spatial harmonic to radiate is that

$$k_0 = \frac{2\pi}{d(1+|\sin\theta|)}, \tag{38}$$

which occurs when the frequency is given by

$$f_c = \frac{c}{d(1+|\sin\theta|)}, \tag{39}$$

so that θ is assumed to be greater than zero below without loss of generality. This condition on the spacing is the same as that required to avoid side lobes in an array with many elements, as noted by Kinsler et al [19] (eqn 7.8.19) for example.

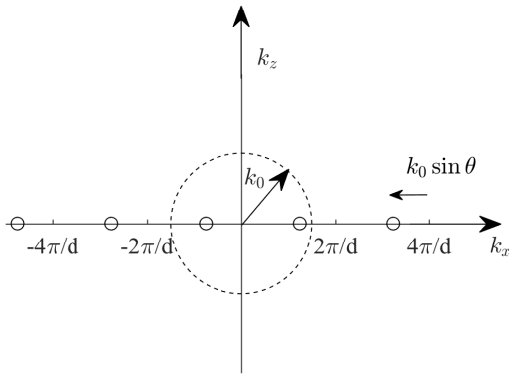

Figure 7: The k-space representation of the wavenumber spectrum for the infinite 2-D array, phased to control plane waves at an angle of θ, where $\circ$ denotes a spatial harmonic. A radiation circle is also plotted, dashed, for a frequency that is slightly below c/d. The spatial harmonics are shifted along the k_x axis from their positions when there is no phasing by a distance of $k_0 \sin\theta$.

The normal velocity distribution due to the secondary source array is now

$$v_s(x,z) = v_s \mathrm{e}^{-\mathrm{j}k_0 x \sin\theta} \left[\mathrm{e}^{-\mathrm{j}k_0 z \cos\theta} + 2\sum_{n=1}^{\infty} \cos(k_{xn}x)\mathrm{e}^{-\mathrm{j}k_{zn}z} \right], \tag{40}$$

where

$$k_{zn} = \sqrt{k_0^2 - (k_{xn} - k_0 \sin\theta)^2}. \tag{41}$$

So if $n = 0$, then $k_{z0} = k_0 \cos\theta$, as expected. The pressure field associated with the secondary source array can again be obtained from the momentum equation as

$$p_s(x,z) = \rho_0 c_0 v_s \mathrm{e}^{-\mathrm{j}k_0 x \sin\theta} \left[\frac{\mathrm{e}^{-\mathrm{j}k_0 z \cos\theta}}{\cos\theta} + 2\sum_{n=1}^{\infty} \frac{k_0}{k_{zn}} \cos(k_{xn}x)\mathrm{e}^{-\mathrm{j}k_{zn}z} \right]. \tag{42}$$

The total normal velocity and pressure distributions, due to both the primary plane wave and the secondary source array are thus

$$\begin{aligned} v_T(x,z) = &\left(\frac{p_p \cos\theta}{\rho_0 c_0} + v_s \right) \mathrm{e}^{-\mathrm{j}k_0(x\sin\theta + z\cos\theta)} + \cdots \\ &2v_s \sum_{n=1}^{\infty} \cos(k_{xn}x)\mathrm{e}^{-\mathrm{j}(k_0 x \sin\theta + k_{zn}z)} \end{aligned} \tag{43}$$

$$\begin{aligned} p_T(x,z) = &\left(p_p + \frac{\rho_0 c_0 v_s}{\cos\theta} \right) \mathrm{e}^{-\mathrm{j}k_0(x\sin\theta + z\cos\theta)} + \cdots \\ &2\rho_0 c_0 v_s \sum_{n=1}^{\infty} \frac{k_0}{k_{zn}} \cos(k_{xn}x)\mathrm{e}^{-\mathrm{j}(k_0 x \sin\theta + k_{zn}z)}. \end{aligned} \tag{44}$$

In this case the cost function, again equal to twice the spatially averaged intensity for this sound field so only the propagating spatial harmonics are considered, is

$$J = \left(p_p^* + \frac{\rho_0 c_0 v_s^*}{\cos\theta} \right) \left(\frac{p_p \cos\theta}{\rho_0 c_0} + v_s \right) + 2\rho_0 c_0 |v_s|^2 \Re \sum_{n=1}^{L} \frac{k_0}{k_{zn}}, \tag{45}$$

where L is again the number of propagating terms. The optimum secondary source strength that minimises J in this case corresponds to

$$v_{s,opt} = \frac{-p_p \cos\theta / \rho_0 c_0}{\left(1 + 2\cos\theta \Re \sum_{n=1}^{L} \frac{k_0}{k_{zn}} \right)}. \tag{46}$$

The optimum source strength is plotted in Figure 8 as a function of the normalised frequency for the cases when θ is equal to 30° and 60°, together with

the attenuation of the primary field in these cases, the number of propagating higher-order spatial harmonics and their wavenumbers. The wavenumbers become real when kd is equal to $2\pi/(1+\sin\theta)$ and have an asymptotic value of $k_0 \cos\theta$ for large values of kd, as expected, but also rise above this asymptotic value, to be equal to k_0 when $k_0 \sin\theta$ is equal to k_{x_n} in eq. (41). It can be seen that the frequency at which perfect control is achieved now drops below c/d Hz, for which d is equal to the acoustic wavelength, towards $c/2d$, for which d is equal to half an acoustic wavelength.

5. Control of plane waves with an infinite array of secondary sources in 3-D

The analysis above for a secondary source array in a 2-D arrangement can be readily extended to the case of an array in a 3-D arrangement. In this case we assume an infinite array of monopole secondary sources in both the x and y directions, as illustrated in Figure 9a. For simplicity, we initially assume a normally incident plane primary wave, as described in Section 2, in which case all the secondary sources must have an equal complex volume velocity, q_s. The normal particle velocity due to the secondary source array is then

$$v_s(x,y) = q_s \sum_{m_1=-\infty}^{\infty} \sum_{m_2=-\infty}^{\infty} \delta(x - m_1 d)\delta(y - m_2 d). \tag{47}$$

The wave number decomposition in this case is

$$v_s(x,y) = v_s \sum_{n_1=0}^{\infty} \sum_{n_2=0}^{\infty} \epsilon_{n_1}\epsilon_{n_2} \cos(k_{x_{n_1}} x)\cos(k_{y_{n_2}} y), \tag{48}$$

where the constant ϵ_{n_1} is defined to be 1 if $n_1 = 0$ and to be 2 if $n_1 > 0$ and ϵ_{n_2} is similarly defined, $v_s = q_s/d^2$, $k_{x_{n_1}} = 2\pi n_1/d$ and $k_{yn_2} = 2\pi n_2/d$. The k-space diagram [10] for this distribution is shown in Figure 9b, and has a regular grid of wave number components with spacing $2\pi/d$. Also shown by the dashed line on this diagram is the radiation circle corresponding to an excitation frequency that is just above c/d, in which case the four (n_1, n_2) higher order wave components $(0, \pm 1)$ and $(\pm 1, 0)$ can all propagate. The four wave number components $(\pm 1, \pm 1)$ cannot propagate at this frequency however, but do propagate at a slightly higher frequency. Figure 10a shows the number of higher-order wave number components that can propagate in

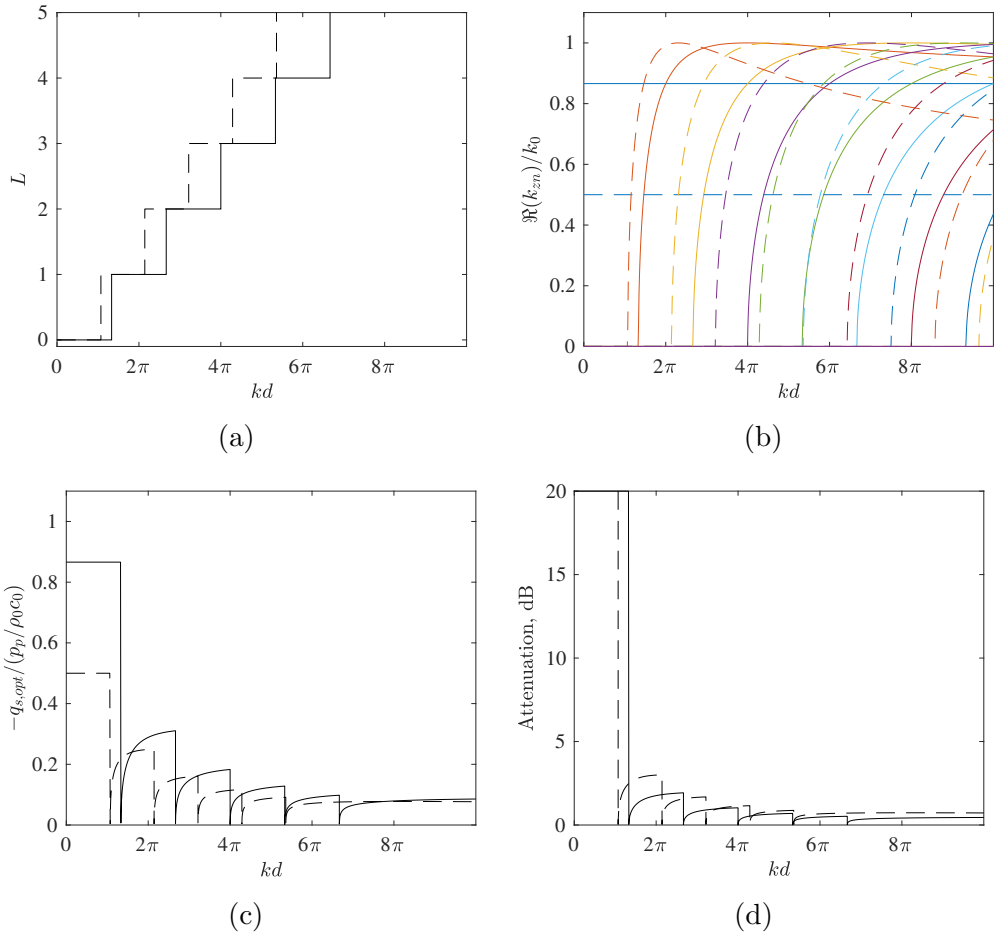

Figure 8: The number of higher-order spatial harmonics that can propagate as a function of non-dimensional frequency kd (a) for steered angles of $\theta = 30°$ (solid lines) and $\theta = 60°$ (dashed lines). The real parts of the corresponding wavenumbers in the propagating direction are shown in (b). Also shown is the variation of the optimal secondary source strength with normalised frequency (c), and the resulting attenuation in the primary field (d).

this case as a function of the normalised frequency kd, together with the real parts of k_{z_n} in Figure 10b. The number of propagating modes is considerably larger than in the 2D case shown in Figure 2a, and, on average, the number of propagating higher-order components becomes proportional to k^2 for large kd, in contrast to the 2-D case where the average value of L is proportional to k, in agreement with the analogous duct case [11].

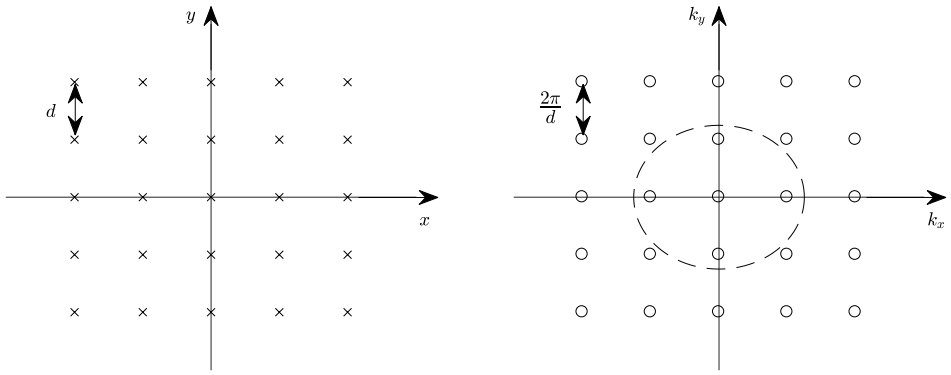

(a) (b)

Figure 9: The physical locations of the secondary monopole sources in the x-y plane for the 3-D case, with a separation of d, (a) and the corresponding k-space diagram, with regular wavenumber components with a separation of $2\pi/d$ (b).

Assuming a normally incident primary plane wave, as in section 2, then the total particle velocity in the 3-D case is now

$$v_T(x,y,z) = \left(\frac{p_p}{\rho_0 c_0} + v_s\right) \mathrm{e}^{-\mathrm{j}k_0 z} + \cdots \\ v_s \left[\sum_{n_1=0}^{\infty}\sum_{n_2=0}^{\infty} \epsilon_{n_1}\epsilon_{n_2} \cos(k_{x_{n_1}} x)\cos(k_{y_{n_2}} y)\mathrm{e}^{-\mathrm{j}k_{z_n} z} - \mathrm{e}^{-\mathrm{j}k_0 z}\right] \quad (49)$$

where the terms in square brackets correspond to the higher order spatial harmonics and now

$$k_{zn} = \sqrt{k_0^2 - k_{x_{n_1}}^2 - k_{y_{n_2}}^2}. \quad (50)$$

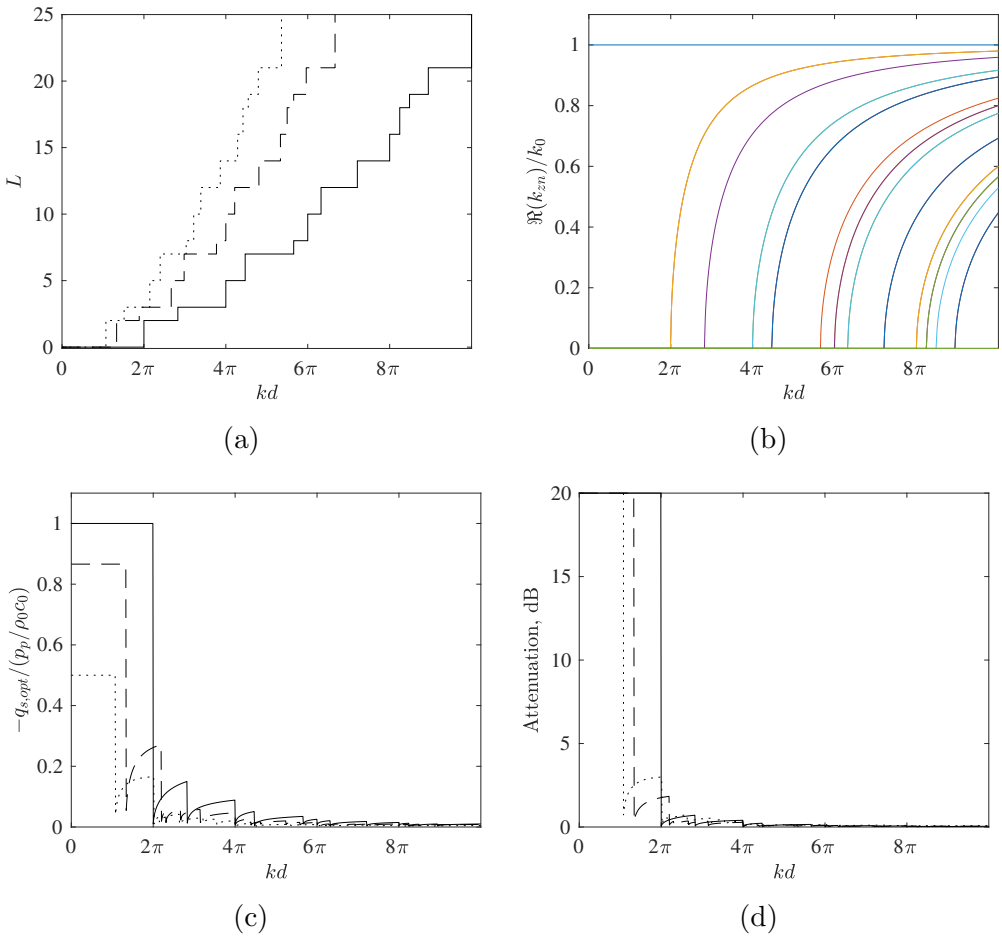

Figure 10: The number of higher-order spatial harmonics that can propagate, L, in the case of the two-dimensional array shown in Fig. 9, as a function of normalised frequency, kd, equal to $2\pi d/\lambda$ (a) for steered angles of $\theta = 0°$ (solid lines), $\theta = 30°$ (dashed lines) and $\theta = 60°$ (dotted lines), together with the real parts of the corresponding wavenumbers in the propagating direction for $\theta = 0°$ only (b). The optimal secondary source velocity is also shown (c) together with the attenuation in the primary field (d) for steered angles of $\theta = 0°$ (solid lines), $\theta = 30°$ (dashed lines) and $\theta = 60°$ (dotted lines).

The corresponding total pressure is

$$p_T(x,z) = (p_p + \rho_0 c_0 v_s)\,\mathrm{e}^{-\mathrm{j}k_0 z} + \cdots \\ \rho_0 c_0 v_s \left[\sum_{n_1=0}^{\infty}\sum_{n_2=0}^{\infty} \epsilon_{n_1}\epsilon_{n_2}\frac{k_0}{k_{z_n}}\cos(k_{xn_1}x)\cos(k_{yn_2}y)\mathrm{e}^{-\mathrm{j}(k_{z_n}z)} - \mathrm{e}^{-\mathrm{j}k_0 z}\right]. \tag{51}$$

The cost function defined above, equal to twice the space averaged acoustic intensity is given in this case by

$$J = \left(p_p^* + \rho_0 c_0 v_s^*\right)\left(\frac{p_p}{\rho_0 c_0} + v_s\right) + \rho_0 c_0 |v_s|^2 \Re \sum_{n=1}^{L} \epsilon_{n_1}\epsilon_{n_2}\frac{k_0}{k_{zn}}, \tag{52}$$

where L is again the total number of propagating higher-order modes.

It is important to note that the first higher-order wave number components in the 3-D case starts to propagate when kd is equal to 2π, i.e. at a frequency of c/d Hz, which is exactly the same as in the 2-D case in Section 2. It is the way that the number of propagating higher-order modes increase with frequency beyond c/d Hz that is different in the two cases.

The optimum secondary source strengths thus correspond in this case to

$$v_{s,opt} = \frac{-p_p/\rho_0 c_0}{\left(1 + \Re\sum_{n=1}^{L}\epsilon_{n_1}\epsilon_{n_2}\frac{k_0}{k_{z_n}}\right)} \tag{53}$$

as also plotted, together with the attenuation in this case, in Figure 10. The attenuation has a similar form to that in the 2-D case, being perfect up to a frequency of c/d Hz, but drops off more rapidly than in the 2-D case for frequencies above this because of the larger number of higher-order wave number components that can propagate in the 3-D case.

In the case of an oblique primary field, at an angle of θ and ϕ, the primary pressure is

$$p_p(x,y,z) = p_p \mathrm{e}^{-\mathrm{j}(k_0 x\sin\theta\cos\phi + k_0 y\sin\theta\sin\phi + k_{z_0}z)} \tag{54}$$

when

$$k_{z_0} = k_0\cos\theta \tag{55}$$

with associated particle velocity, normal to the array, of

$$v_p(x,y,z) = \frac{p_p}{\rho_0 c_0}\mathrm{e}^{-\mathrm{j}(k_0 x\sin\theta\cos\phi + k_0 y\sin\theta\sin\phi + k_{z_0}z)}. \tag{56}$$

To control this the normal velocity of the secondary source array must be phased such that

$$v_s(x,y,z) = q_s \sum_{m_1=-\infty}^{\infty} \sum_{m_2=-\infty}^{\infty} \delta(x-m_1 d)\delta(y-m_2 d) \mathrm{e}^{-\mathrm{j}k_0 d(m_1 \sin\theta\cos\phi + m_2 \sin\theta\sin\phi)} \tag{57}$$

so that the wave number spectrum becomes

$$v_s(x,y,z) = v_s \mathrm{e}^{-\mathrm{j}k_0(x\sin\theta\cos\phi + y\sin\theta\sin\phi)} \left[\sum_{n_1=0}^{\infty} \sum_{n_2=0}^{\infty} \epsilon_{n_1}\epsilon_{n_2} \cos(k_{x_{n_1}} x) \cos(k_{y_{n_2}} y) \right] \tag{58}$$

The wave number components in the k-space diagram are now shifted with respected to both the k_x and k_y axes compared with the case in Figure 9b. The analysis of the performance follows from Section 4 and that above, so that the optimum source strength now corresponds to

$$v_{s,opt} = \frac{-p_p \cos\theta / \rho_0 c_0}{\left(1 + \cos\theta \Re \sum_{n=1}^{L} \epsilon_{n_1}\epsilon_{n_2} \frac{k_0}{k_{z_n}}\right)} \tag{59}$$

where in this case

$$k_{z_n} = \sqrt{k_0^2 - (k_{x_{n_1}} - k_0 \sin\theta\cos\phi)^2 - (k_{y_{n_2}} - k_0 \sin\theta\sin\phi)^2}. \tag{60}$$

This secondary source strength and the corresponding attenuation are also plotted in Figure 10 for the case in which $\theta = 30^\circ$ and $\theta = 60^\circ$.

6. Control of plane waves transmitted through a finite aperture

To analyse the physical limits of the active control of a plane wave transmitted through a finite aperture, the two-dimensional geometry shown in Figure 11 is used, and the acoustic field is calculated using a 2-D finite-element model (FEM). Although it may be possible to analyse the diffracting effects of a finite aperture analytically, this is not straightforward. The spatial windowing methods described in [20], for example, cannot be used directly since it is found that the velocity distribution across the aperture is not just a spatially-windowed version of that in the free field, as the particle velocity around the edges of the aperture is increased due to the diffraction of the incident wave and the scattered field in the opposite direction [21]. The

sound field is also complicated by the thickness of the wall and so for convenience numerical methods have been used in the first instance. The spatial resolution in the simulation plane is set to be one-sixth the wavelength of the highest frequency of interest, 4 kHz. The primary noise to be controlled is an incident plane wave, as above, but in this case it is transmitted through the finite aperture. It is initially assumed to be travelling in the z-direction, at $\theta = 0°$. An array of N secondary line sources is used, and the sources nearest to the edges are a distance of $d/2$ from the edge of the aperture [6]. When $N = 1$, the source is placed at the centre of the aperture and d is set equal to $w/2$, where w is the overall size of the aperture in Figure 11.

The active control problem in this case [22] can be formulated in terms of minimising a cost function equal to the sum of squared pressures, which in this case are calculated at 1100 evaluation points on an arc 5 m away from the centre of the window, that is itself 2 m across, as shown in Figure 11. The cost function is given by

$$J = \mathbf{e}^H\mathbf{e} + \beta\mathbf{q}_s^H\mathbf{q}_s = \mathbf{q}_s^H\mathbf{A}\mathbf{q}_s + \mathbf{q}_s^H\mathbf{b} + \mathbf{b}^H\mathbf{q}_s + \mathbf{d}^H\mathbf{d}, \tag{61}$$

where $\mathbf{e} = \mathbf{d} + \mathbf{G}\mathbf{q}$, is the vector of complex pressures at the evaluation points, $\mathbf{d}$ is the vector of disturbance signals due to the incident plane wave at these points, $\mathbf{G}$ is the matrix of plant responses between the secondary sources and the pressure evaluation points, $\mathbf{q}_s$ is the vector of secondary source strengths. The superscript H denotes the Hermitian of the matrix, i.e. the complex conjugate transpose and β is a regularisation parameter [22]. Hence, after substitution, $\mathbf{A} = \mathbf{G}^H\mathbf{G} + \beta\mathbf{I}$ and $\mathbf{b} = \mathbf{G}^H\mathbf{d}$.

The resulting optimal secondary source strengths are given by

$$\mathbf{q}_{s,opt} = -\left[\mathbf{G}^H\mathbf{G} + \beta\mathbf{I}\right]^{-1}\mathbf{G}^H\mathbf{d}. \tag{62}$$

The regularisation parameter is chosen to avoid ill-conditioning with respect to the calculation of the inverse of the matrix $\mathbf{G}^H\mathbf{G}$, but has little effect on the control performance for the values used in these simulations.

The resulting attenuations of the cost function, predicted from of the FEM simulations, are shown in Figure 12 for different numbers of secondary sources, N, in the plane of the aperture. The results are plotted as a function of the normalised frequency, both when it is normalised to the size of the aperture, kw in Figure 12a, and when it is normalised on the separation distance between the sources, kd in Figure 12b. The results in Figure 12a correspond to the practical case, in which the size of the aperture corresponds

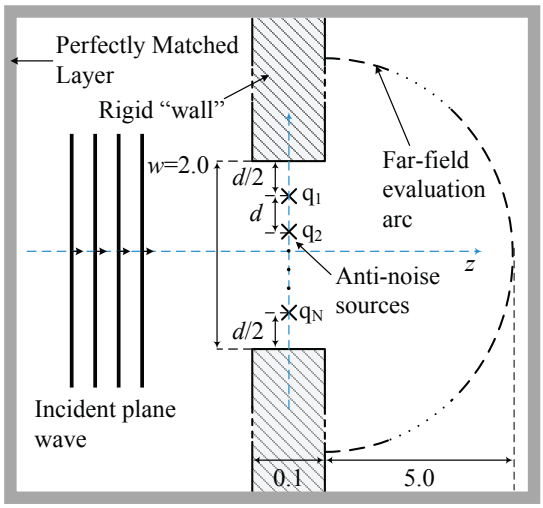

Figure 11: Finite element model geometry for the active control of a plane wave through a finite aperture with a finite linear array of secondary line sources in 2-D.

to that of a window, which is fixed, and the excitation frequency is then increased. The performance clearly increases as the number of secondary sources is increased, as expected, but it is not clear whether this is entirely because these sources are closer together, or whether there is also an effect due to diffraction, which will be more important at low frequencies than at high frequencies. This question is resolved in Figure 12b, which corresponds to the case in which the size of the aperture is increased as the number of sources becomes larger, and is consistent with the analytical representation used in the previous sections. It can be seen in Figure 12b that when the number of sources is large, the results approximate those for the infinite case, in Figure 2d, with significant levels of attenuation being achieved up to frequencies of $f = c_0/d$, which corresponds to a normalised frequency of $kd = 2\pi$. When only a few sources are used, the performance is not as great, indicating that diffraction has a significant effect, although there is still some sign of the cut-off frequency effect seen in the infinite case.

Simulations have also been performed for oblique incidence waves, and an example set of results for 13 sources is shown in Figure 13. Although the change in the cut-on frequency seen in the simulation results of Figure 8d is not quite so clear, the simulation results do indicate that the upper frequency of control is reduced, as predicted by eq. (39).

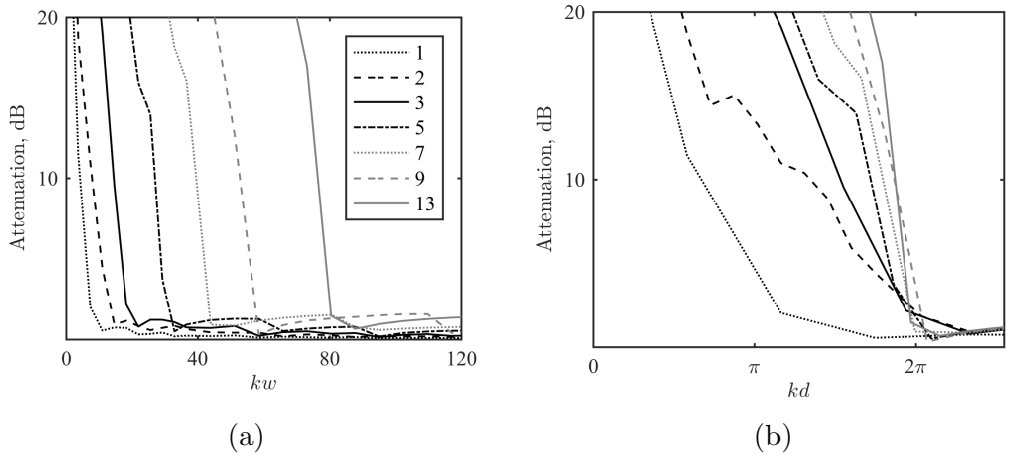

Figure 12: Attenuation of far-field pressure in the finite element simulations with a normally-incident plane wave, plotted as a function of frequency, normalised both by the size of the aperture, kw in Figure 12a, and when normalised by the separation between the sources, kd in Figure 12b, for different numbers of secondary sources.

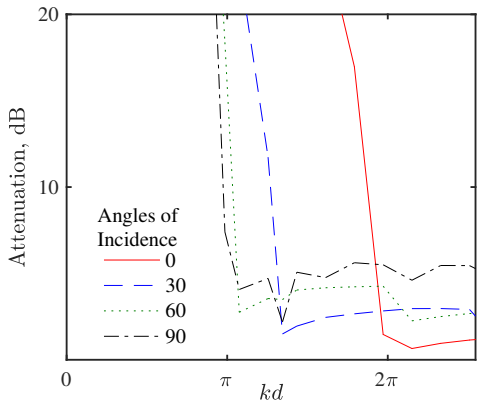

Figure 13: Attenuation of the far-field pressure in the finite element simulations with 13 sources and for different angles of incidence of the primary plane wave, plotted as a function of frequency normalised by the separation between the sources, kd.

Finally, Figure 14 shows the distributions of the sound pressure level, normalised to that of the incident wave, after control with 5 secondary sources in the geometry of Figure 11. The results are shown for excitation frequencies corresponding to source separation distances of 0.5λ and 0.9λ, in order to be comparable with the corresponding free field results in Figure 3. It can be seen that in the lower frequency case shown in Figure 14a, when d is equal to 0.5λ, the pressure distribution is similar to that in the free field case, so that the guidelines on the placement of the error microphones discussed in Section 3 are still valid. For the higher frequency excitation, corresponding to d equal to 0.9λ, however, the near field generated by the secondary sources and the diffracted incident wave is considerably more complicated in Figure 14b than it is for the free field case, and the evanescent components of the pressure distribution do not decay away as rapidly. It is perhaps not surprising that the sound field beyond the aperture is more intense, since it can be seen from Figure 12b that the attenuation in the radiated power is only about 10 dB in this case, and good attenuation at this frequency requires more than just 5 secondary sources.

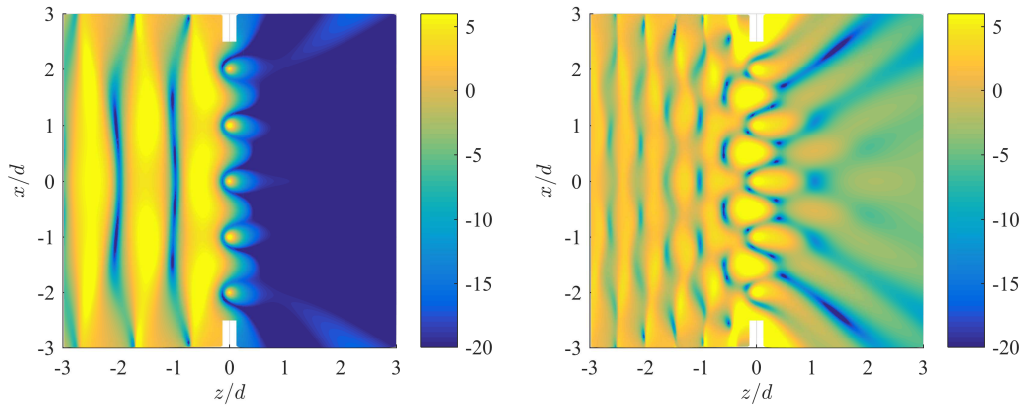

Figure 14: The sound pressure level, in dB relative to the incident pressure, after active control of an incident plane wave transmitted through the aperture shown in Figure 11 with 5 secondary sources, for $k_0 d$ equal to π (a) and 1.8π (b) corresponding to source separation distances of 0.5λ and 0.9λ.

7. Conclusions

A wavenumber approach has been used to analyse the active control of an incident plane wave with an infinite array of secondary sources. It is found that perfect control of a normally-incident plane wave can be achieved in the far field, provided the separation between the uniformly-spaced secondary sources is less than the acoustic wavelength, i.e. at frequencies of less than $f = c_0/d$. This is found to be the case both for a 1-D array of line sources in a 2D analysis, and also for a 2-D array of monopoles in a 3-D analysis.

For oblique angles of incidence, the upper frequency of control is reduced. For a grazing wave the upper frequency of control is $f = c_0/2d$, which corresponds to the separation between the sources being half a wavelength. The near-field of these sources is also analysed, which provides guidance on the placement of the error microphones in a practical arrangement. At frequencies for which the source separation distance is less than half a wavelength, placing the error microphones at a distance of greater than about half the source separation distance should ensure good active control performance.

A numerical simulation of active control is then performed for the active control of a plane wave after transmission through an aperture in a rigid wall, with an array of secondary sources in the aperture, which has practical applications for the reduction of sound through open windows. When there are many secondary sources, and the size of the aperture is large compared with the wavelength, so that diffraction is not so important, significant attenuations in far field power are again found for frequencies up to $f = c_0/d$. When the size the aperture is not large compared with the wavelength and diffraction becomes more important, a smaller number of secondary sources are required but the attenuation is then not as good as in the free field case when plotted as a function of kd. It is also found that the near field pressure in this case is similar to that in the free field when the source separation is less than half a wavelength, but that this becomes more complicated and intense at higher frequencies, indicating that greater care is required in the placement of error microphones in this case.

References

[1] M. Zavadskaya, A. Popov, B. Egelskii, An approximate solution of the problem of active suppresion of sound fields by the malyuzhinets method, Soviet Physics Acoustics-USSR 21 (6) (1976) 541–544.

[2] S. Konyaev, V. Lebedev, M. Fedoryuk, Discrete approximation of a spherical huygens surface, Soviet Physics Acoustics-USSR 23 (4) (1977) 373–374.

[3] G. Mangiante, Active sound absorption, The Journal of the Acoustical Society of America 61 (6) (1977) 1516–1523.

[4] P. Nelson, S. Elliott, Active control of sound, Academic, New York, 1992.

[5] T. Murao, M. Nishimura, Basic study on active acoustic shielding, Journal of Environment and Engineering 7 (1) (2012) 76–91.

[6] B. Lam, S. Elliott, J. Cheer, W.-S. Gan, The physical limits of active noise control of open windows, in: 12th Western Pacific Acoustics Conference, Singapore, 2015.

[7] S. Wang, J. Yu, X. Qiu, M. Pawelczyk, A. Shaid, L. Wang, Active sound radiation control with secondary sources at the edge of the opening, Applied Acoustics 117 (2017) 173–179.

[8] S. Elliott, J. Cheer, B. Lam, C. Shi, W.-S. Gan, Controlling incident sound fields with source arrays in free space and through apertures, in: Proceedings of the 24th International Congress on Sound and Vibration, 2017.

[9] P. Doak, Excitation, transmission and radiation of sound from source distributions in hard-walled ducts of finite length (i): The effects of duct cross-section geometry and source distribution space-time pattern, Journal of Sound and Vibration 31 (1) (1973) 1–72.

[10] E. G. Williams, Fourier acoustics: sound radiation and nearfield acoustical holography, Academic press, 1999.

[11] P. M. Morse, K. U. Ingard, Theoretical acoustics, Princeton university press, 1968.

[12] S. Spors, R. Rabenstein, Spatial aliasing artifacts produced by linear and circular loudspeaker arrays used for wave field synthesis, in: 120th AES Convention, Citeseer, 2006.

[13] S. Spors, J. Ahrens, Spatial sampling artifacts of wave field synthesis for the reproduction of virtual point sources, in: Audio Engineering Society Convention 126, Audio Engineering Society, 2009.

[14] S. J. Elliott, J. Cheer, H. Murfet, K. R. Holland, Minimally radiating sources for personal audio, The Journal of the Acoustical Society of America 128 (4) (2010) 1721–1728.

[15] H. F. Olson, Modern sound reproduction, Van Nostrand Reinhold, 1972.

[16] T. J. Holmes, The acoustic resistance box - a fresh look at an old principle, Journal of the Audio Engineering Society 34 (12) (1986) 981–989.

[17] J. Cheer, Designing loudspeaker directivity for mobile devices, Master's thesis, University of Southampton, UK (2009).

[18] M. F. Simón Gálvez, S. J. Elliott, J. Cheer, A superdirective array of phase shift sources, The Journal of the Acoustical Society of America 132 (2) (2012) 746–756.

[19] A. Kinsler, L. Frey, A. B. Coppens, J. V. Sanders, Fundamentals of acoustics (2001).

[20] M. Villot, C. Guigou, L. Gagliardini, Predicting the acoustical radiation of finite size multi-layered structures by applying spatial windowing on infinite structures, Journal of sound and vibration 245 (3) (2001) 433–455.

[21] K. Hongo, H. Serizawa, Diffraction of an acoustic plane wave by a rectangular hole in an infinitely large rigid screen, The Journal of the Acoustical Society of America 106 (1) (1999) 29–35.

[22] S. J. Elliott, Signal Processing for Active Control, Academic Press, London, 2001.